

Egocentric Human-Object Interaction Detection: A New Benchmark and Method

Kunyuan Deng ^{✉a}, Yi Wang ^{✉a} and Lap-Pui Chau ^{✉a,*}

^aDepartment of Electrical and Electronic Engineering, The Hong Kong Polytechnic University, Hong Kong SAR

ARTICLE INFO

Keywords:

Egocentric vision
Human-object interaction
HOI detection
Interaction recognition

ABSTRACT

Understanding the interaction between humans and objects has gained much attention in recent years. Existing human-object interaction (HOI) detection methods mainly focus on the third-person perspectives, overlooking a more intuitive way from the egocentric view of HOI, namely Ego-HOI. This paper introduces an Ego-HOIBench, a new dataset to promote the benchmarking and development of Ego-HOI detection. Our Ego-HOIBench comprises more than 27K egocentric images with high-quality hand-verb-object triplet annotations across 123 fine-grained interaction categories and locations, covering a rich diversity of scenarios, object types, and hand configurations in daily activities. In addition, we explore and adapt third-person HOI detection methods to Ego-HOIBench and illustrate the challenges of hand-occluded objects and the complexity of single- and two-hand interactions. To build a new baseline, we propose a Hand Geometry and Interactivity Refinement (HGIR) scheme, which leverages hand pose and geometric information as valuable cues for interpreting interactions. Specifically, the HGIR scheme explicitly extracts global hand geometric features from the estimated hand pose proposals and refines the interaction-specific features using pose-interaction attention. This scheme enables the model to obtain a robust and powerful interaction representation, significantly improving the Ego-HOI detection capability. Our approach is lightweight and effective, and it can be easily applied to HOI baselines in a plug-and-play manner to achieve state-of-the-art results on Ego-HOIBench. Our project is available at: <https://dengkunyuan.github.io/EgoHOIBench/>

1. Introduction

Egocentric human-object interaction (Ego-HOI) detection aims to locate interacting human-object pairs and reason about their interaction relationships from the first-person vision. As a crucial task in human-centered advanced scene understanding, its precise outcomes can drive advancements in a wide range of downstream applications, including embodied intelligence [1, 2, 3], mixed reality [4, 5], surveillance event detection [6, 7], and visual question answering [8, 9, 10]. By analyzing images captured from a first-person perspective, the Ego-HOI assistance system offers guidance and feedback based on the user's actions, facilitating tasks such as cooking and assembly. Furthermore, this technology has the potential to enhance embodied intelligence in imitation learning and the execution of complex tasks.

HOI detection has made significant progress in third-person vision [11, 12, 13, 14, 15, 16, 17, 18, 19]. However, it is rarely explored from the egocentric view. The primary reason is the lack of benchmark datasets clearly labeled for the Ego-HOI detection task. On the one hand, the significant domain mismatch between the HOI datasets captured from third-person vision and the egocentric task renders them unsuitable for direct application to Ego-HOI detection. As shown in Fig. 1, the third-person perspective (top row) provides a comprehensive view of the human body posture and surroundings, while the egocentric perspective (bottom row) captures interaction details of hands and objects in close range. On the other hand, although a large number of egocentric datasets have emerged in recent years, e.g., Ego4D



Figure 1: Examples of human-object interactions from third-person perspective (top row) and egocentric perspective (bottom row). Different colors represent distinct elements of each HOI triplet <human/hand, verb, object>.

[20], EPIC-KITCHENS[21, 22], they usually focus on the action recognition task and lack high-quality fine-grained annotations of three fundamental elements of Ego-HOI: <human hand, verb, object>. Furthermore, these datasets either only cover a single scene [22, 23, 24, 25, 26, 27] or single-hand interactions [28], or focus on rigid objects with relatively simple interaction patterns but ignore articulated objects [24, 25, 26, 28, 29], which is far from sufficient for building a comprehensive understanding of egocentric human-object interactions in real-world scenarios. The limitations of existing egocentric public datasets regarding annotation modalities and interaction diversity severely hinder the development of Ego-HOI detection.

*Corresponding author

✉ lap-pui.chau@polyu.edu.hk (Lap-Pui Chau)

The narrow field of view in egocentric vision leads to severe visual occlusion [29, 30, 31], presenting a significant challenge for interaction recognition. Existing HOI detection methods are usually designed for third-person vision and rely on the rich contextual information provided by the broad view of external cameras. When applied to egocentric vision, these methods suffer from the loss of information due to mutual occlusions of hands and objects, affecting their performance in Ego-HOI detection. Due to the structural connectivity properties of human skeletons, human pose features exhibit higher robustness and reliability than traditional visual features when dealing with partial occlusions [32, 33, 34]. Based on this insight, previous studies [11, 34, 35, 36, 37, 38, 39] have attempted to incorporate pose information to distinguish subtle interaction differences. However, these methods usually depend on human pose estimators or body part detectors, which is unsuitable for hand posture estimation in egocentric scenes. Moreover, they primarily focus on extracting geometric features from the overall structure of the human body, which are not specifically designed for hands. Therefore, it is crucial to further explore flexible and effective ways to capture gesture cues to facilitate egocentric interactivity learning even under occlusion.

In view of the above issues, **1)** we present a new benchmark dataset, Ego-HOIBench, featuring explicit and high-quality <human hand, verb, object> triplet annotations to facilitate research on Ego-HOI perception. Our dataset covers 27,575 images and 123 hand-verb-object triplet categories, thoroughly annotating the bounding boxes and categories of human hands, active objects, and their relations. It not only extensively covers diverse hand-object interaction scenarios but also includes and distinguishes single-hand and two-hand manipulated interactions. We also define two Ego-HOIBench challenges under instance-level and image-level settings to explore the Ego-HOI detection task. **2)** We propose a lightweight and effective interaction enhancement scheme, Hand Geometry and Interactivity Refinement (HGIR), that utilizes hand pose and geometric cues to improve the interaction representations from a global perspective. In particular, our approach first estimates multiple sets of candidate hand joint positions based on hand features from an HOI baseline detector. Then, we construct global hand geometric features by designing a selection strategy to identify the most suitable hand pose proposals. Next, we enhance interaction representation by pose prompts with pose-interaction attention, generating pose-aware interaction features. Finally, hand geometric features and pose-aware interaction features are fused for interaction recognition. Note that our method can be flexibly integrated with off-the-shelf HOI detectors, eliminating the need for additional hand pose estimators and achieving impressive efficiency. The main contributions of our work can be summarized as follows:

- We introduce an Ego-HOIBench, the first Ego-HOI detection benchmark containing 27K real-world egocentric images and 123 fine-grained hand-verb-object

triplet annotations. Besides, we adapt and reimplement four representative third-person HOI detection methods on Ego-HOIBench, aiming to significantly advance the benchmarking works in egocentric interactive localization and recognition research.

- We propose a plug-and-play interaction enhancement scheme, i.e. HGIR, incorporating global hand pose understanding to complement and enhance interaction representations in the egocentric vision. Our approach is lightweight, effective, and general and works seamlessly with off-the-shelf HOI detection methods.
- Experiments in representative and influential HOI baselines with our scheme validate its significant performance improvements. Extensive experiments, ablation studies, and discussions are conducted to illustrate the significance of benchmarking EgoHOI.

2. Related Work

2.1. Egocentric Datasets and Benchmarks

With the development of wearable devices and smart glasses, increasing egocentric datasets have been proposed to study human activities from the unique first-person viewpoint [8, 20, 21, 22, 23, 24, 25, 26, 27, 28, 29, 30, 40, 41, 42]. Here, we focus on datasets related to interaction perception and localization. EPIC-KITCHENS and its extensions [21, 22] are a series of large-scale datasets that capture long-term unscripted activities in kitchen environments and densely label actions through an automatic annotation pipeline. To comprehensively study attention and action, EGTEA Gaze+ [23] records video and audio of meal preparation tasks and simultaneously provides gaze tracking, hand masks, and fine-grained action annotations. Compared with any other datasets, Ego4D [20] has a massive scale and unprecedented diversity. It builds a vast suite of benchmarks, including episodic memory, hands and objects, audio-visual diarization, social interaction, and forecasting. Datasets and benchmarks such as these fill the gaps in the first-person vision for different visual perception tasks, such as action recognition, video captioning, and hand detection.

However, most works focus on action recognition or custom tasks and do not provide joint annotations of <human hand, verb, object> required for training and evaluating Ego-HOI detection models. Many datasets [22, 30] detail all objects interacting with the hand over time but do not explicitly specify the current active object, which is essential for constructing Ego-HOI annotations. Although the MEC-CANO dataset [25] provides clear and complete Ego-HOI annotations, it only considers toy assembly activities. Such a limited scenario is very detrimental to the generalization of the Ego-HOI detection model. Furthermore, object diversity is essential in fully understanding interactions, but some datasets [24, 25, 26, 28, 29] tend to collect behavioral data related to rigid objects with simple interactions, ignoring articulated objects. The diversity of hand configurations is also often overlooked. The FPHA dataset [28] only presents

Table 1

Comparison of Ego-HOIBench with existing egocentric datasets. Active Object Distinction denotes that the annotation specifies the object involved in the current interaction. Hand Dist. means distinguishing between left and right hands. (*): It can be converted from masks. (**): Only available for a subset of frames.

Dataset	Scenario	Modality	Real	#Interactions/ Actions	#Nouns	#Verbs	Object BBs	Active Object Distinction	Arti- culated	Hand BBs	Hand Poses	Hand Dist.	Year
<i>Single Scenario</i>													
EGTEA Gaze+ [23]	Kitchens	RGB	✓	106	53	19	×	×	✓	*	×	×	2018
EPIC-KITCHENS-100 [22]	Kitchens	RGB	✓	4,053	300	97	✓	×	✓	✓	×	✓	2020
Assembly101 [24]	Toy assembly	RGB	✓	1,380	90	24	×	×	×	×	✓	N/A	2022
MECCANO [25]	Toy assembly	RGB-D	✓	61	20	12	✓	✓	×	✓	×	✓	2022
AssemblyHands [26]	Toy assembly	RGB	✓	N/A	N/A	6	×	×	×	×	✓	✓	2023
EgoISM-HOI [27]	Industrial-like	RGB-D	×	N/A	19	2	✓	✓	✓	✓	×	✓	2024
<i>Multiple Scenarios</i>													
FPHA [28]	Daily activities	RGB-D	✓	45	26	N/A	×	N/A	×	×	✓	×	2018
H2O [29]	Daily activities	RGB-D	✓	36	8	11	✓	N/A	×	×	✓	✓	2021
Ego4D [20]	Multi-domain	RGB	✓	N/A	87 ¹	74 ¹	✓	N/A	N/A	**	×	✓	2022
HOI4D [30]	Daily activities	RGB-D	✓	N/A	16	22	*	×	✓	*	✓	✓	2022
Ego-HOIBench (Ours)	Daily activities	RGB-D	✓	123	22	18	✓	✓	✓	✓	✓	✓	2024

¹ This number is obtained from the "Short-Term Object Interaction Anticipation" task.

² Most images are synthetic.

the 3D joint locations for right hands, while H2O [29] focuses on two-hand operations. Although some datasets [23, 28] cover both single-hand and two-hand interactions, they do not consider differentiating between the left and right hands. These oversights hinder a comprehensive understanding of interactions under different hand configurations. In addition, although recent egocentric datasets have primarily focused on videos, image-based Ego-HOI detection remains highly novel and valuable for research. It is particularly well-suited for resource-limited devices and real-time applications due to its easy accessibility, fast response, and low computational requirements. The comparison between our work and existing public datasets is shown in Table 1. To the best of our knowledge, our Ego-HOIBench is the first real image-based dataset that comprises explicit and high-quality annotations of <human hand, verb, object> for Ego-HOI detection, covering a rich set of scenarios, objects, and hand configurations.

2.2. HOI Detection

In recent years, HOI detection has attracted widespread research interest. This task aims to gain a fine-grained understanding of human activities by localizing human-object pairs and inferring their high-level semantic relationships. Existing HOI detection work can be categorized into two- and one-stage methods based on their detection strategies. The two-stage methods [11, 13, 15, 35, 36, 38, 43, 44, 45, 46, 47, 48] involve using a frozen object detector (e.g., FasterRCNN [49], DETR [50]) to generate proposals for human-object pairs. These proposals are then classified using a separate network based on the features of cropped regions. The two-stage methods usually extract additional visual and contextual information, such as spatial [43, 45, 48], language [13, 15], and human pose features [11, 35, 36, 38], to improve interaction representations. Some studies [43, 47] also utilize graph structures for message propagation between detected human and object instances, thereby enhancing

the reasoning performance of interactions between these instance nodes. Decoupling the stages enables training solely the interaction recognition network, thereby saving computational resources and improving training efficiency. However, optimizing the two sub-problems separately may result in suboptimal results. In contrast, the one-stage methods [16, 17, 51, 52, 53, 54, 55] directly detect HOI triplets from the entire image. Early CNN-based one-stage methods use interaction points [51] or union boxes [53] to predict interactions, but these heuristics rely on complex post-processing techniques such as Non-Maximum Suppression. Building on the success of DETR [50] in object detection, many approaches have extended the Transformer architecture to achieve end-to-end HOI detection [16, 17, 52, 54]. According to the degree of decoupling of human detection, object recognition, and interaction recognition, these methods can be further divided into single-branch [17, 56], two-branch [52], and three-branch [54] methods. Overall, these methods benefit from the strengths of Transformers in efficiently capturing long-range dependencies and have achieved significant performance improvements.

2.3. Human Pose as HOI Cues

Recognizing the importance of human pose in understanding human behavior and intention, researchers have explored various methods [11, 34, 35, 36, 37, 38, 57, 58] to extract and leverage pose features to enhance interaction representations. For example, Park *et al.* [11] designed a pose-conditioned graph neural network that utilizes local features of human joints to update human node encoding to contain richer local information. Qiao *et al.* [34] focused on extracting geometric features, such as human posture and object position, to supplement visual features to improve robustness in partially occluded scenes. Li *et al.* [35] emphasized the unique characteristics of human body parts related to interactivity and proposed a hierarchical learning framework based on instance-level and part-level body features. However, these works mainly focus on the local pose features

of the target person, neglecting global clues from other people in the image. To overcome this limitation, Wu *et al.* [58] introduced body-part saliency maps to capture multi-person features and learn the overall relationship between different body parts. Nevertheless, most of these methods rely on off-the-shelf human pose estimators or body part detectors, significantly increasing complexity and computational costs. Moreover, these models are typically trained on third-person datasets, making their application challenging in first-person scenarios. To address these issues, our work leverages the geometric robustness of global hand pose features to provide crucial complementary information to visual features, deepening our understanding of the complex dynamics of Ego-HOI under partial occlusion. We integrate hand pose estimation into our Ego-HOI detection pipeline, sharing weights with the hand detection branch. This integration not only addresses generalization limitations but also reduces the computational burden, making the entire system more efficient and practical.

3. Our Ego-HOIBench Benchmark

Ego-HOIBench is an egocentric image dataset explicitly annotated for Ego-HOI detection research. The dataset provides high-quality ground truth annotations for hand-object pair detection and interaction recognition across all frames. Hand and object annotations contain multiple (*class*, *bbox*) tuples, where *class* indicates the hand side (left or right) or object category, and *bbox* denotes a bounding box determined by the coordinates of its top-left and bottom-right corners. Interaction annotations specify the exact action category performed by each hand-object pair. Combined with original hand pose annotations, our Ego-HOIBench dataset provides rich details for studying human-object interactions in egocentric vision.

3.1. Generation Steps

We perform the following steps to acquire images and generate annotations for our Ego-HOIBench benchmark. Given an untrimmed RGB-D video sequence derived from the HOI4D dataset [30], we begin by extracting the intermediate frames from each action clip, based on the identified start and end timestamps, as these frames effectively capture sufficient information. Then, the intermediate frame's mask regions are associated with the corresponding object categories. According to the definition of the Ego-HOI detection task, we focus only on the active objects in current frames. By analyzing the task information, we restrict the possible categories of active objects and filter out irrelevant objects. To avoid meaningless component segmentation, we merge different components of the same objects, e.g., the scissors' left and right parts, and the safe's body and door. Subsequently, we convert the mask regions into bounding boxes. A hand-object pair's bounding boxes and categories are combined with the corresponding action category to form a complete Ego-HOI triplet annotation, i.e., <human hand, verb, object>. Since subtle errors in pixel-level masks can lead to considerable deviations in corresponding bounding

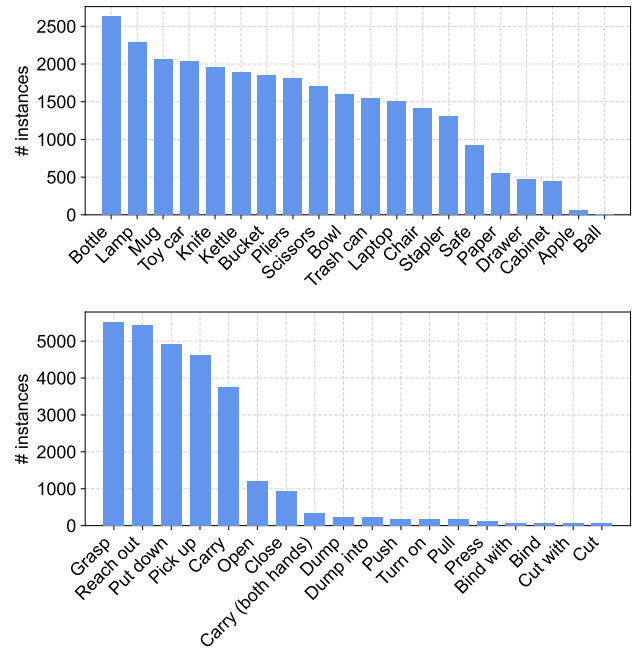


Figure 2: Distributions of objects (top) and verbs (bottom), sorted by instance count. Some categories appear significantly more frequently than others.

boxes, we employ human experts to double-check and ensure accurate annotations. The label correction work is time-consuming, requiring a combined effort of twenty person-days. The entire dataset generation process spans approximately one and a half months. The extracted intermediate frames and their annotations constitute the Ego-HOIBench dataset. The Ego-HOIBench dataset is further divided into training and test sets. We split the frames according to their video identities to ensure no overlap of object entities in the training and test sets. With a split ratio of 80%:20%, we finally obtain 22,088 training frames and 5,487 testing frames.

3.2. Dataset Statistics

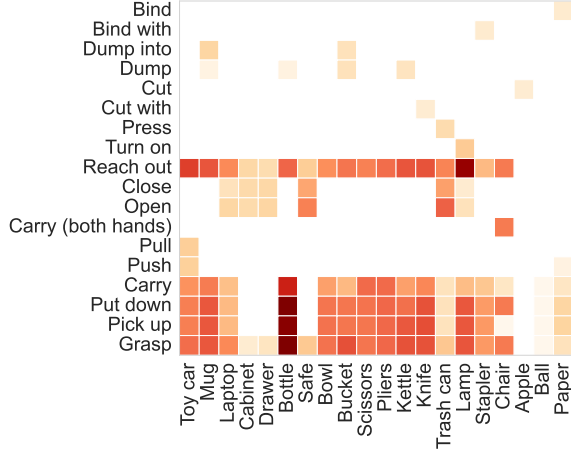
The Ego-HOIBench dataset contains 27,575 RGB-D frames, with a frame resolution of 1920×1080. It covers 22 representative noun classes, including 10 rigid object classes and 10 articulated object classes, as well as left-hand and right-hand categories. We annotate 58.4K bounding boxes, with ~28K for objects. We consider 18 different verbs to describe actions typically performed by camera wearers in daily activities, ensuring broad coverage of common types. *Grasp, Pick up, Put down, Carry, Push, Pull, Carry (both hands), Open, Close, Reach out, Turn on, Press, Cut with, Cut, Dump, Dump into, Bind with, Bind.*

Among the observed instances, the vast majority (91.4%) rely on the right hand alone, while fewer cases (8.2%) use both hands. Even fewer cases operate with the left hand alone, accounting for only 0.4%. Fig. 2 shows the distributions of object and verb categories under the instance-level setting, the definition of which will be illustrated in

Table 2

Statistics of instances and Ego-HOI triplet categories at different occlusion ratios in our Ego-HOIBench Dataset.

Split	#Frames	#Total Ins.	#Instances					#Triplet Categories				
			@0~0.2	@0.2~0.4	@0.4~0.6	@0.6~0.8	@0.8~1	@0~0.2	@0.2~0.4	@0.4~0.6	@0.6~0.8	@0.8~1
Train	22,088	22,481	12,235	5,600	2,756	1,193	697	107	105	93	62	42
Test	5,487	5,567	3,090	1,344	656	325	152	100	96	75	50	20

**Figure 3:** Co-occurrence of verbs and objects. The darker color of the block indicates a higher number of corresponding instances.

Sec. 3.3. The instance number of different object categories show a significant span, ranging from 2630 to 8. This wide distribution range is also reflected in the number of verbs. The triplet combination of hands, verbs, and objects further exacerbates the data imbalance, reflecting the natural distribution of HOIs in the real world. This characteristic makes Ego-HOIBench a distinctive and challenging benchmark for Ego-HOI detection, presenting challenges that are closely related to practical applications.

Fig. 3 shows the co-occurrence between verbs and objects (e.g., *Open* and *Drawer*). Each square in the heat map directly reflects the number of instances involving a particular verb-object pair, with darker colors indicating more corresponding instances. Our dataset contains various distinctive co-occurrence scenes, where some specific verbs, such as *Turn on* only associated with the object *Lamp*, and *Press* only co-occurs with *Trash can*. The co-occurrence between objects (including hands) and verbs highlights the feasibility of using this information to suppress negative prediction candidates. This suppression scheme closely mirrors human decision-making processes and is therefore frequently employed during the model inference stage [11, 43].

Table 2 provides detailed statistics on the number of instances and Ego-HOI triplet categories at various occlusion ratios for the training and test sets in our Ego-HOIBench dataset. The occlusion ratio of an Ego-HOI instance is calculated by dividing the area of the object occluded by hands and other objects by the area of its bounding box. In our dataset, occlusion is common, with roughly half of the instances having at least 20% of their area occluded and about

20% having an occlusion ratio over 40%. The high occlusion ratios increase the difficulty of detection and recognition and affect the model's generalization and robustness. In addition, the number of triplet categories decreases significantly as occlusion increases. This phenomenon is closely related to the physical size of the objects. Larger objects, such as cabinets and chairs, are typically only slightly obscured by hands or other objects. In contrast, smaller objects, like staplers and bowls, are more prone to varying degrees of occlusion.

3.3. Ego-HOI Detection Tasks

Following a third-person perspective, HOI is defined as a triplet containing a person, a verb, and an object [14, 59]. It assumes a one-to-one correspondence between these three elements. Since people, as interacting subjects, remain constant, most HOI detection models disregard subject identification but focus solely on the localization of humans. In the context of egocentric vision, Ragusa *et al.* [25] described interactions with multiple objects using $\langle \text{verb}, \text{objects} \rangle$, completely ignoring the role of the human hand in the interaction. However, a person's left and right hands can independently perform different interactions or collaborate on a single interaction, making it an oversimplification to treat a person's hands as a single, unchanging entity. Furthermore, human hands are not passive in activities but actively influence and shape the nature of interactions. Therefore, a comprehensive understanding of hand factors is indispensable for Ego-HOI detection.

Building upon the aforementioned understanding, we redefine Ego-HOI as the $\langle \text{hands}, \text{verb}, \text{objects} \rangle$ triplet. We emphasize the significance of hands in interactions and consider comprehending their categories and positions as essential for understanding egocentric interaction dynamics. In light of the definition of Ego-HOI, we present two detection tasks to evaluate the model's capacity to comprehend interactions at the instance level and the abstract image level.

3.3.1. Instance-level Ego-HOI Detection Task

Let $\mathcal{H} = \{h_r, h_l\}$, $\mathcal{V} = \{v_1, v_2, \dots, v_m\}$, and $\mathcal{O} = \{o_1, o_2, \dots, o_n\}$ denote the sets of hands, verbs, and objects, respectively, where m and n are the number of verbs' and objects' categories, respectively. We define the prediction target for each instance as follows:

$$ehoi_{ins} = \left\{ \left(\overline{h_r}, \overline{h_l} \right), v_i, o_j \right\} \quad (1)$$

where $\left(\overline{h_r}, \overline{h_l} \right)$ are the hands engaged in the interaction. There are three situations to consider: right hand only (h_r, \cdot) ,



Figure 4: Examples of general, instance-level specific, and image-level specific hand-object interactions. The instance-level setting focuses on the interaction behaviors involving a single active object, while the image-level setting interprets the interaction holistically from the perspective of the entire image. In the instance-level setting (second row), an image may be parsed into two separate interaction instances: *right-hand bind paper* and *right-hand bind with stapler*. In contrast, the image-level setting (last row) defines the image as a unified interaction: *right-hand bind paper with stapler*. For clarity, the hand category is omitted from the image captions.

left hand only (\cdot, h_l) , and both hands (h_r, h_l) . $v_i \in \mathcal{V}$ is the verb that describes interaction, and $o_j \in \mathcal{O}$ is the object of interest. The annotations for each instance comprise the class labels for the hand(s) and active object, along with their respective bounding boxes and the verb class label. In total, we define 123 Ego-HOI triplet categories consisting of one or two hands, a verb, and an object, e.g., *right-hand cut apple* and *left and right hands dump bucket*.

3.3.2. Image-level Ego-HOI Detection Task

The objective of image-level Ego-HOI detection is to deduce the primary interaction within each frame and identify all hands and active objects participating in it. Compared with the instance-level setting, the image-level setting comprehensively considers the objects directly and indirectly involved in the interaction when analyzing triplets. For example, in the instance-level setting, an image may be parsed into two separate interaction instances *right-hand bind paper* and *right-hand bind with stapler*. In contrast, the image-level setting defines the image as a unified interaction *right-hand bind paper with stapler*. This image-level perspective examines and explains interaction behaviors from a broader perspective. To explain the instance-level and image-level Ego-HOI detection tasks more clearly, we show examples of hand-object interactions in Fig. 4.

4. Our Method

In this work, we present a Hand Geometry and Interactivity Refinement (HGIR) scheme that enhances interaction learning in Ego-HOI detection by leveraging global hand

pose cues. Our method comprises four components: the hand pose estimation block for obtaining hand pose candidates (see Sec. 4.2 for details), the hand geometry extraction block that focuses on exploiting global structural features (see Sec. 4.3 for details), the interactivity refinement block by optimizing pose-interaction attention (see Sec. 4.4 for details), and the feature aggregation block for fusing complementary geometric and refined interaction features (see Sec. 4.5 for details).

4.1. HGIR Architecture

Our HGIR scheme is straightforward yet robust and can be easily integrated with various baseline HOI detection methods, yielding appealing results in the Ego-HOI detection task. The overall architecture of our method is shown in Fig. 5.

Given an input RGB image $\mathbf{X} \in \mathbb{R}^{H \times W \times 3}$, we employ the original baseline HOI detection method to obtain the hand features $\mathbf{H} \in \mathbb{R}^{N \times d}$, the object features $\mathbf{O} \in \mathbb{R}^{N \times d}$, and the interaction features $\mathbf{I} \in \mathbb{R}^{N \times d}$, denoted as $(\mathbf{H}, \mathbf{O}, \mathbf{I}) = \text{Baseline}(\mathbf{X})$. The baseline method can adopt either a unified or decoupled prediction strategy as long as it provides the necessary interaction (i.e., verb) and hand (i.e., subject) representations. Multiple hand pose candidates $\hat{\mathcal{G}} \in \mathbb{R}^{N \times 2N_g}$ are estimated based on \mathbf{H} , where N_g is the number of hand joints. Then, a selection strategy is designed to generate left-hand and right-hand pose proposals, and their geometric features $\mathbf{f} \in \mathbb{R}^{2KN_g(N_g-1)}$ are extracted to describe the details of hand structure. Simultaneously, the interactivity refinement block uses the attention mechanism to direct the interaction features focus toward the regional

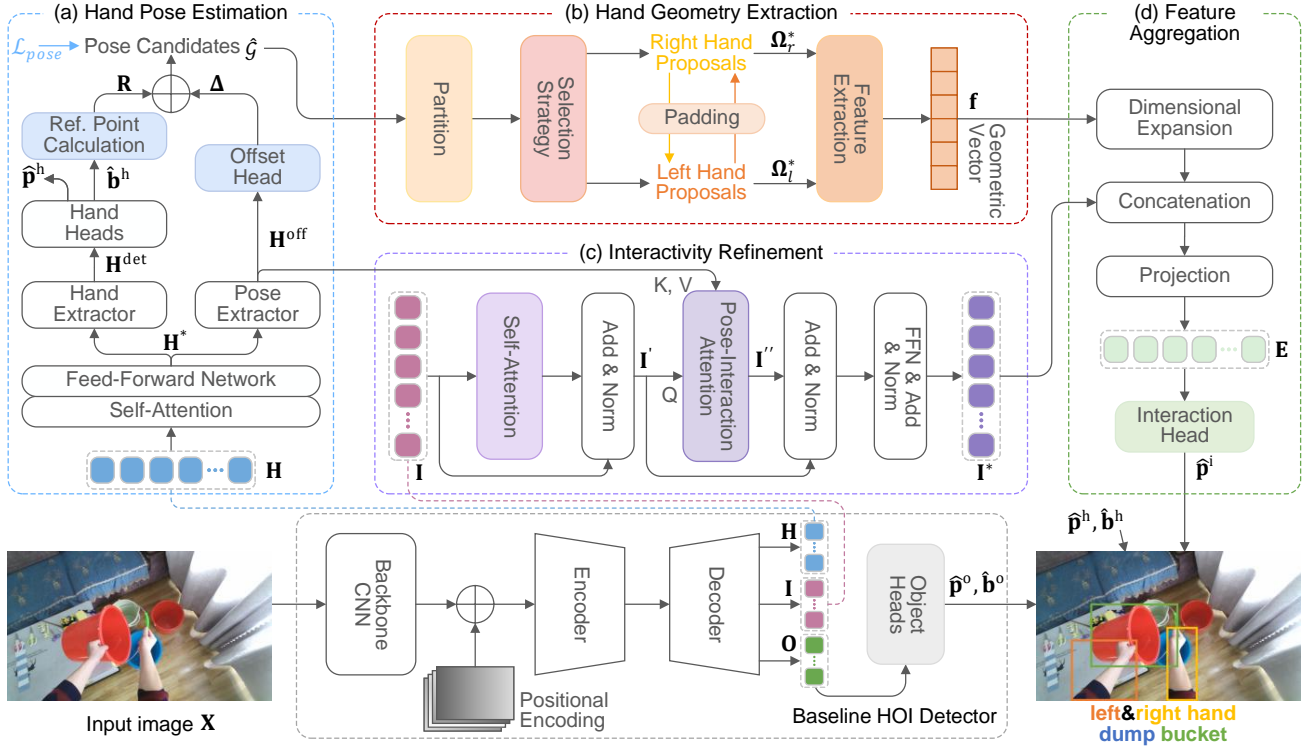


Figure 5: Overview of our framework. Given an input image, a baseline HOI detection method (at the bottom) generates the initial hand (\mathbf{H}), object (\mathbf{O}), and interaction (\mathbf{I}) features. (a) Within our HGIR scheme (at the top), a set of pose candidates ($\hat{\mathcal{G}}$) is first estimated based on \mathbf{H} (see Sec. 4.2). (b) Top K pairs of hand proposals are then selected, and their geometric features (\mathbf{f}) are further extracted to reveal the dynamic structural properties of hands in interactions (see Sec. 4.3). (c) Simultaneously, the hand pose offset-specific prompts (\mathbf{H}^{off}) are incorporated to enrich the interaction representations using the pose-interaction attention mechanism (see Sec. 4.4). (d) Finally, the hand geometric features and refined pose-aware interaction features (\mathbf{I}^*) are aggregated to obtain enhanced interaction embedding (\mathbf{E}) for interaction recognition (see Sec. 4.5). Our scheme is dedicated to interactivity learning and can be integrated with baseline HOI methods that provide interaction and hand features.

information derived from pose offset prompts \mathbf{H}^{off} . These two features are fused to obtain the ultimate interaction embedding $\mathbf{E} \in \mathbb{R}^{N \times d}$ for classification. Overall, our HGIR scheme exploits the synergy of complementary geometric features and refined interaction features to enhance the ability to perceive interaction dynamics.

4.2. Hand Pose Estimation

Our pose estimation block embeds the auxiliary task of hand pose estimation into the HOI baseline method, sharing most of the network and weights with the hand detection branch. This strategy minimizes computational overhead and allows for flexible adaptation to different datasets without being restricted by the domain of the external hand pose estimator.

Some HOI baseline methods offer specialized hand features, while others use instance features to uniformly describe both the subject and object. To extract and emphasize hand information more deeply, we apply a consistent Transformer encoder across various baseline methods. This encoder is primarily composed of a self-attention layer and a feed-forward (FFN) layer. Formally, we obtain the advanced hand representations using this encoder, denoted as $\mathbf{H}^* = \text{Encoder}(\mathbf{H})$, where \mathbf{H}^* consists of N vectors $\mathbf{h}_i \in \mathbb{R}^d$.

Two lightweight multi-layer perceptrons (MLP) are then used in parallel to extract hand detection-specific features \mathbf{H}^{det} and pose offset-specific features \mathbf{H}^{off} , where i -th feature vectors are calculated as $\mathbf{h}_i^{\text{det}} = \text{MLP}(\mathbf{h}_i)$ and $\mathbf{h}_i^{\text{off}} = \text{MLP}(\mathbf{h}_i)$, respectively. Here, the main reason for choosing MLPs as feature extractors is to ensure the feature index alignment. This index consistency lays the foundation for the subsequent combination of in-box reference points and pose offsets according to the shared indexes.

Reference Point. Two small FFNs f_{hc} , f_{hb} are adopted as prediction heads to obtain the hand classification probabilities $\{\hat{\mathbf{p}}_i^h\}_{i=1}^N$ (i.e., left hand or right hand) and bounding boxes $\{\hat{\mathbf{b}}_i^h\}_{i=1}^N$ of all N tokens, respectively, as follows:

$$\begin{aligned} \hat{\mathbf{p}}_i^h &= \delta(f_{hc}(\mathbf{h}_i^{\text{det}})) \in \mathbb{R}^{|\mathcal{H}|+1} \\ \hat{\mathbf{b}}_i^h &= \sigma(f_{hb}(\mathbf{h}_i^{\text{det}})) \in \mathbb{R}^4 \end{aligned} \quad (2)$$

where δ and σ are the sigmoid and softmax operations, respectively. $|\mathcal{H}|$ denotes the number of hand category set, and the additional class represents the background class (no object). The predicted category \hat{c}_i^h and score \hat{s}_i^h are given by $\arg \max_k \hat{\mathbf{p}}_{i,k}^h$ and $\max_k \hat{\mathbf{p}}_{i,k}^h$.

Using the predicted N hand bounding boxes, we determine the reference points $\mathbf{R} = \{(xref_i, yref_i)\}_{i=1}^N$. After in-depth analysis and experimental verification, we choose the top center point of each bounding box as the reference point, which constrains the positions of hand joint points to the vicinity of the hand, making it easier to obtain accurate estimates of joint positions.

Offset. Using an additional offset head, we predict the offsets of $N_g = 21$ hand joints relative to the corresponding reference point from \mathbf{R} along the x and y axes. Taking the hand offset-specific features as inputs, the i -th offset vector predicted by the offset head f_Δ is given by:

$$\Delta_i = \sigma(f_\Delta(\mathbf{h}_i^{\text{off}})) \in \mathbb{R}^{2N_g} \quad (3)$$

where $\{(\Delta_{i,2k-1}, \Delta_{i,2k}) \mid k = 1, \dots, N_g\}$ denotes the x -coordinate and y -coordinate of the k -th joint.

The reference points and offsets of the same indexes are added to obtain a set of hand gesture candidates $\hat{\mathcal{G}} = \{\hat{\mathbf{g}}_i \mid \hat{\mathbf{g}}_i \in \mathbb{R}^{2N_g}\}_{i=1}^N$, as follows:

$$(\hat{\mathbf{g}}_{i,2k-1}, \hat{\mathbf{g}}_{i,2k}) = (xref_i + \Delta_{i,2k-1}, yref_i + \Delta_{i,2k}) \quad (4)$$

where $k \in \{1, \dots, N_g\}$.

Combining reference points and offsets instead of directly predicting joint positions offers two key advantages. Firstly, it avoids the complexity of directly finding joint points from the entire image. Secondly, the pose offset-specific features can act as valuable prompts in the subsequent interactivity refinement.

4.3. Hand Geometry Extraction

From an egocentric view, the hands can carry out tasks independently or collaboratively. Even though the left and right hands perform different actions, they can still provide valuable complementary information to each other. Therefore, we extract the geometric features of all hands in the image from a global perspective based on the pose estimation results to gain a comprehensive insight into the interaction's semantics.

Selection Strategy. We match the hand pose candidates with predicted hand categories and scores to obtain a set of $\{(\hat{\mathbf{g}}_i, \hat{c}_i^h, \hat{s}_i^h)\}_{i=1}^N$. This matching process also benefits from the index consistency mentioned before. Based on \hat{c}_i^h , the hand pose candidates are partitioned into two sets $\Omega = \{\Omega_l, \Omega_r\}$, where Ω_l and Ω_r denote the set of predictions whose categories are left hand and right hand, respectively.

To screen out high-quality hand pose candidates, we preset a threshold T_{pose} and the retained left-hand and right-hand pose candidates are denoted as $\Omega'_l = \{\hat{\mathbf{g}}_i \in \Omega_l \mid \hat{s}_i^h \geq T_{pose}\}$ and $\Omega'_r = \{\hat{\mathbf{g}}_i \in \Omega_r \mid \hat{s}_i^h \geq T_{pose}\}$, respectively. For each set, we re-rank the candidates based on \hat{s}_i^h and select the Top K candidates with the highest confidence to constitute the pose proposals. In the case of fewer than K valid candidates, we use the candidates of the other hand for padding to maintain feature integrity. For example, if the number of

valid candidates for the left hand is less than K , we will use candidates from the right hand for padding, and vice versa:

$$\begin{aligned} \Omega_l^* &= \Omega'_l \cup \left\{ \hat{\mathbf{g}}_i \in \Omega'_r \mid i = 1, \dots, K - |\Omega'_l| \right\} \\ \Omega_r^* &= \Omega'_r \cup \left\{ \hat{\mathbf{g}}_i \in \Omega'_l \mid i = 1, \dots, K - |\Omega'_r| \right\} \end{aligned} \quad (5)$$

where $|\cdot|$ indicates the number of the set. In this manner, regardless of the number of valid candidates, the final sets Ω_l^* and Ω_r^* will each contain exactly K proposals.

Geometric Feature Extraction. The angles between joints are critical to intuitively reflecting hand-related interactions. Based on this understanding, we extract joint geometric features from the left- and right-hand pose proposals. Formally, for the i -th proposal, the feature vector consisting of directional components of all non-repeated joint pairs is as follows:

$$\mathbf{f}_i^\tau = [dx_{jk}, dy_{jk} \mid \forall j, k \in \{1, \dots, N_g\}, j < k] \quad (6)$$

where $\tau \in \{l, r\}$ denotes the left-hand and right-hand proposals, respectively. And $dx_{jk} = \frac{\hat{\mathbf{g}}_{i,2k-1} - \hat{\mathbf{g}}_{i,2j-1}}{\|\hat{\mathbf{g}}_{i,2k-1} - \hat{\mathbf{g}}_{i,2j-1}\|}$ and $dy_{jk} = \frac{\hat{\mathbf{g}}_{i,2k} - \hat{\mathbf{g}}_{i,2j}}{\|\hat{\mathbf{g}}_{i,2k} - \hat{\mathbf{g}}_{i,2j}\|}$ are the normalized directional components on the x - and y -axis of the j -th and k -th joint pairs, respectively. By concatenating all the features of the left and right proposals, we obtain a global geometric vector, given by:

$$\mathbf{f} = [\mathbf{f}_1^l; \dots; \mathbf{f}_K^l; \mathbf{f}_1^r; \dots; \mathbf{f}_K^r] \quad (7)$$

\mathbf{f} is a $2KN_g(N_g - 1)$ -dimensional vector, which not only captures rich inter-joint clues but also enhances our understanding of hand interactivity through gesture contexts from both hands.

4.4. Interactivity Refinement

To obtain pose-aware interaction representations, we introduce hand pose prompts to refine the interaction-specific features using a pose-interaction attention mechanism.

The refiner contains a self-attention layer [50] that focuses on capturing and modeling the intrinsic correlations within the interaction features, obtaining the advanced interaction features $\mathbf{I}' = \{\mathbf{I}'_i\}_{i=1}^N$. Next, we introduce the pose offset-specific features \mathbf{H}^{off} as pose prompts to inject pose awareness into the advanced interaction features. Specifically, we feed \mathbf{H}^{off} into the attention mechanism as keys and values, while \mathbf{I}' serves as queries. Each output element \mathbf{I}_i'' is computed by aggregating all values weighted with attention: $\mathbf{I}_i'' = \sum_j \alpha_{ij} (\mathbf{W}_v \mathbf{h}_j^{\text{off}})$, where α_{ij} is the normalized attention weight, as follows:

$$\alpha_{ij} = \text{softmax} \left(\frac{(\mathbf{W}_q \mathbf{I}'_i)^T \mathbf{W}_k \mathbf{h}_j^{\text{off}}}{\sqrt{d}} \right) \quad (8)$$

where $\mathbf{W}_q, \mathbf{W}_k, \mathbf{W}_v$ are learnable embedding matrices corresponding to queries, keys, and values, respectively. After

passing \mathbf{I}' through the subsequent FFN layer, we finally obtain the refined pose-aware interaction representations \mathbf{I}^* . Our refiner contains only one decoder layer without consuming many computational resources. In this way, we guide the interaction features to focus on regions and features that are closely related to the subtle changes in hand poses.

4.5. Feature Aggregation

To make the perception of interactivity more robust and effective, we aggregate the global hand geometric features \mathbf{f} and the refined pose-aware interaction features $\mathbf{I}^* \in \mathbb{R}^{N \times d}$.

First, the dimensions of both need to be aligned. To this end, we take a straightforward method: expand the dimensions of the feature vector \mathbf{f} by repeating N times. Next, we concatenate the tiled geometric feature map and the interaction features, and project them into a unified embedding space using an MLP. The feature aggregation can be formulated as follows:

$$\mathbf{E} = f_{emb}(\text{Concat}[\mathbf{I}^*, \text{Tile}(\mathbf{f})]) \quad (9)$$

Using the enhanced embedding \mathbf{E} as input to the interaction head significantly improves the model's performance compared to using only the refined interaction features \mathbf{I}^* . This improvement is attributed to the effective fusion of hand geometry and pose-aware interaction features, which complement each other and enhance the Ego-HOI detection model's reasoning about interactive behaviors.

4.6. Training and Inference

In addition to the hand bounding box and category prediction heads mentioned in Eq. 2, our method employs another three heads to predict the verb category, object category, and object bounding box.

Training Objective. The baseline HOI detection methods are usually trained using a multi-task loss, as follows:

$$\mathcal{L}_{base} = \lambda_{L1} \mathcal{L}_{L1} + \lambda_{GIoU} \mathcal{L}_{GIoU} + \lambda_{hoc} (\mathcal{L}_{oc} + \mathcal{L}_{hc}) + \lambda_{ac} \mathcal{L}_{ac} \quad (10)$$

where L1 loss [49] \mathcal{L}_{L1} and GIoU loss [60] \mathcal{L}_{GIoU} are applied to both hand and object bounding box regression, and focal loss [61] \mathcal{L}_{ac} is for interaction classification. Notably, the Ego-HOI detection task considers hand classification, which differs from the third-person perspective. Therefore, the cross-entropy loss is employed not only for object classification \mathcal{L}_{oc} , but also for hand classification \mathcal{L}_{hc} . λ_{L1} , λ_{GIoU} , λ_{hoc} and λ_{ac} are the hyper-parameters for weighting each loss. The loss functions of the baseline models [54, 56] and comparison models [46, 52] are similar to Eq. 10, but the details may be different due to the unique characteristics of each model.

The learning of auxiliary hand pose estimation is supervised by the average L1 loss, as follows:

$$\mathcal{L}_{pose} = \frac{1}{2N_g} \sum_{i=1}^N \sum_{j=1}^{2N_g} |\mathbf{g}_{i,j} - \hat{\mathbf{g}}_{i,j}| \quad (11)$$

where $\mathbf{g}_{i,j}$ and $\hat{\mathbf{g}}_{i,j}$ are the ground truth and prediction result of the j -th value of the i -th hand pose candidate, respectively.

During training, the original loss \mathcal{L}_{base} is integrated with the auxiliary pose estimation loss in Eq. 11. The overall loss \mathcal{L} is given by:

$$\mathcal{L} = \mathcal{L}_{base} + \lambda_{pose} \mathcal{L}_{pose} \quad (12)$$

where the weight λ_{pose} denotes the weight to balance \mathcal{L}_{base} and \mathcal{L}_{pose} , and is 1.0 by default.

Inference. Given a set of Ego-HOI prediction results $\{(\hat{\mathbf{p}}_i^i, \hat{\mathbf{p}}_i^h, \hat{\mathbf{p}}_i^o, \hat{\mathbf{b}}_i^h, \hat{\mathbf{b}}_i^o)\}_{i=1}^N$, where $\hat{\mathbf{p}}_i^i \in \mathbb{R}^{|\mathcal{V}|}$ and $\hat{\mathbf{p}}_i^o \in \mathbb{R}^{|\mathcal{O}|+1}$ correspond to the classification probabilities for interaction and object respectively, the predicted category c_i^τ and its score s_i^τ are given by $\arg \max_k \hat{\mathbf{p}}_{i,k}^\tau$ and $\max_k \hat{\mathbf{p}}_{i,k}^\tau$. Considering the hand classification, the confidence score of an Ego-HOI prediction is defined as follows:

$$s_i^{ehoi} = s_i^i \cdot s_i^h \cdot s_i^o \quad (13)$$

And we only select the top several predictions with confidence scores above a threshold from all N results.

5. Experiments

5.1. Integration to Off-the-shelf HOI Detectors

Our method is general and can be seamlessly integrated with most existing HOI detection approaches. The integration process is straightforward. In this work, we select two representative yet diverse baseline methods to evaluate the effectiveness of our proposed approach thoroughly.

MUREN [54] is an end-to-end Transformer-based approach with a three-branch architecture. It decouples human detection, object detection, and interaction classification, using independent decoder layers to extract task-specific tokens for sub-task learning. In our integration, the interaction branch's attention fusion module output is leveraged as the interaction representations \mathbf{I} , while the human branch's attention fusion module output serves as the hand representations \mathbf{H} .

QPIC [56] is one of the pioneering Transformer-based set prediction models for HOI detection. It employs a single decoder to predict all three elements of HOI: human, verb, and object. In our integration, the unified features output by the decoder are used indiscriminately as the original interaction features \mathbf{I} and hand features \mathbf{H} . We apply a vanilla encoder to the unified features to derive the object-specific features.

5.2. Experimental Setup

Implementation Details. Our experiments cover two baselines and their integrations with our method. We also include other existing HOI detection methods for comparison, all of which are modified and retrained for the Ego-HOI detection task. Our experimental and analytical endeavors focus on the instance-level setting, as this level provides richer details. Image-level detection can be achieved by simply modifying the prediction heads or post-processing,

Table 3

Performance and efficiency comparison of different HOI baselines with and without integration with our method. For clarity, all AP and Accuracy metrics are presented as percentages.

Method	Backbone	Ego-HOIBench				Efficiency	
		mAP ₅₀ ↑	mAP ₇₅ ↑	Full ↑	Top@G Acc. ↑	#Params ↓	FPS ↑
MUREN [54]	ResNet-50	83.5	75.6	65.0	81.4	75M	15.9
+ Ours	ResNet-50	84.1	76.3	66.8(+1.8)	85.7(+4.3)	79M(+4M)	15.0(-5.7%)
QPIC [56]	ResNet-101	84.8	80.8	76.7	86.5	60M	18.6
+ Ours	ResNet-101	85.9	83.4	78.4(+1.7)	92.7(+6.2)	65M(+5M)	17.1(-8.1%)

so we do not compare them here. To obtain better detection performance, we fine-tune the object detector (usually DETR [50] with a ResNet-50 backbone) on the Ego-HOIBench training set. All experiments are performed on 4 RTX 4090 GPUs. The hyper-parameters in the experiment remain consistent with the default settings of respective methods, but the batch size and initial learning rate are adjusted according to the supported computing resources. Specifically, all experiments of HOTR [52] and MUREN [54] adopt a batch size of 16 and an initial learning rate of $5e-5$. For STIP [46], the HOI detector with a frozen object detector uses a batch size of 16 and an initial learning rate of $5e-5$, while the batch size is 8 and the initial learning rate is $1e-5$ during the two-stage joint fine-tuning. QPIC [56] is trained with a batch size of 8 and an initial learning rate of $5e-5$.

Evaluation Metrics. We evaluate models' performance on the Ego-HOIBench benchmark using mean average precision (mAP) with IoU thresholds ranging from 0.5 to 0.95 with a step size of 0.05. A detection result is considered a true positive only if the predicted hand, object, and verb categories are all correct, and the hand and object bounding boxes have IoUs with ground truths larger than the specified threshold. We further divide all the Ego-HOI triplet categories into rare and non-rare according to whether they appear at least 100 times in the training set. Based on this criterion, we report the mAP for the Full, Rare, and Non-rare categories. The mAPs of the full testing set at IoU thresholds of 0.5 and 0.75 are reported separately, denoted as mAP₅₀ and mAP₇₅, similar to [44, 54]. In addition, to highlight the improvement of our method in interaction recognition, we introduce Top@G Verb Accuracy as a metric. For an image to be considered correct, the G predictions with the highest probabilities must completely cover the set of true verb labels, where G represents the number of true labels.

5.3. Improvement on Two Different Baselines

Table 3 shows the performance comparison of two mainstream baseline HOI detection methods before and after integrating our proposed method. By incorporating our approach, both baseline methods achieve significant performance improvements. Specifically, MUREN [54] achieves a 1.8% improvement in Full mAP and a 4.3% increase in Top@G Accuracy. As for QPIC [56], Full mAP is improved

by 1.7% and Top@G Accuracy obtains a substantial improvement of 6.2%, setting a new high for the state-of-the-art results. These results demonstrate that our method is applicable not only to models with a unified decoder but also to the methods that decouple the sub-tasks. Moreover, our scheme imposes no specific restrictions on the backbone. Note that after integrating our module, these two baseline methods can still maintain end-to-end training and reasoning. We also compare their model sizes and runtime efficiencies to prove that the performance improvement is not due to the increase in model size. Although our method adds several million parameters, this increase is very limited relative to the original model size. Furthermore, in terms of Frames Per Second (FPS), the runtime speed drop is negligible, only a few percentage points. The results show that our technology is extremely lightweight and efficient.

5.4. Comparison with State-of-the-art Methods

Table 4 presents a detailed performance comparison between our proposed method and many typical approaches, including the one-stage single-branch method QPIC [56], the one-stage two-branch method HOTR [52], the one-stage three-branch method MUREN [54], the two-stage method STIP [46] and its jointly fine-tuned version. Here, all AP and Accuracy metrics are presented in percentage form. We use QPIC as the baseline and integrate it with our scheme for comparison. Our method (last row) surpasses all existing one-stage and two-stage methods, whether in Ego-HOI detection or interaction recognition. A noteworthy phenomenon is that the rare triplet categories consistently underperform compared to the non-rare categories in terms of mAP across all other methods. In contrast, our method significantly enhances the detection performance of rare categories, even surpassing that of non-rare categories. The superior performance of our method is mainly due to the fact that we effectively extract and incorporate hand pose cues into the interaction embedding. This enhancement significantly boosts the model's ability to distinguish complex and rare-seen interactions, further improving the overall performance of Ego-HOI detection.

5.5. Ablation Study

We conduct various ablation studies to validate the effectiveness of our method. For each ablation experiment, we modify one hyper-parameter or component while keeping all other hyper-parameters in their optimal settings. The

Table 4

Performance comparison of our proposed method (last row) and state-of-the-art methods on the Ego-HOIBench dataset. All metrics are presented as percentages. † denotes that the object detector and HOI detector are further fine-tuned jointly.

Method	Backbone	End-to-End	Ego-HOI Detection					Interaction Recognition	
			mAP ₅₀	mAP ₇₅	Full	Rare	Non-Rare	Top@G	Accuracy
HOTR [52]	ResNet-50	✓	44.3	18.9	22.4	9.8	27.3		85.1
STIP [46]	ResNet-50	×	47.7	22.4	25.0	10.8	30.4		76.0
STIP† [46]	ResNet-50	×	57.9	30.6	32.1	15.9	38.4		78.4
MUREN [54]	ResNet-50	✓	83.5	75.6	65.0	61.6	66.3		81.4
QPIC [56]	ResNet-50	✓	84.4	78.7	69.5	67.6	70.3		87.4
QPIC [56]	ResNet-101	✓	84.8	80.8	76.7	75.5	77.1		86.5
QPIC + <i>Ours</i>	ResNet-101	✓	85.9	83.4	78.4	79.8	77.9		92.7

Table 5

Ablation study of each component in our HGIR scheme, starting from the baseline and progressively building up to our complete method. ✓ means that the corresponding component is used. HPE: Hand Pose Estimation. IR: Interactivity Refinement. HGE: Hand Geometry Extraction.

HPE	IR	PGE	mAP ₅₀	Full	Top@G Acc.
-	-	-	83.5	65.0	81.4
✓	-	-	83.4	66.0	81.3
✓	✓	-	83.6	66.1	84.7
✓	✓	✓	84.1	66.8	85.7

MUREN baseline is used across all our ablation studies. We choose mAP₅₀, Full mAP, and Top@G Accuracy as representative metrics to evaluate the performance of each variant.

Components of HGIR Scheme. To thoroughly assess the impact of each component in our method, we conduct an ablation study by gradually incorporating them into the baseline. The components evaluated include Hand Pose Estimation (HPE), Interactivity Refinement (IR), and Hand Geometry Extraction (HGE). The results are summarized in Table 5. Compared with the baseline, introducing a supervised HPE block results in a relative Full mAP gain of 1.0%. This gain indicate that the auxiliary task enhances the learning of hand features, which indirectly positively impacts Ego-HOI detection. Next, integrating the IR block yields further advancements. While the gains in mAP₅₀ and Full mAP are relatively modest, Top@G Accuracy achieves a significant leap to 84.7%, with an increase of 3.4%. These performance improvements show that incorporating pose prompts for engaging in meaningful interactions can significantly boost expressiveness.

Our complete method, as shown in the last row of Table 5, which includes the above two components and the PGE component, achieves notable improvements across all three metrics. Specifically, mAP₅₀ is further increased by 0.5%, and Full mAP is significantly improved by 0.7%, and Top@G Accuracy by 1.0%. These results demonstrate

Table 6

Performance comparison of different hand pose estimation schemes.

	Method	mAP ₅₀	Full	Top@G Acc.
(a)	Direct	82.9	65.7	85.3
(b)	Learnable Point	83.1	66.6	85.3
(c)	Center Point	83.6	66.5	84.3
(d)	Top-Center Point	84.1	66.8	85.7

that the extracted hand geometric features provide complementary information, significantly enhancing interaction recognition and detection. The enhancements observed in this ablation study confirm the synergy of each component within the HGIR scheme and highlight the importance of utilizing hand geometric and refined interaction features to improve the model’s accuracy and robustness in Ego-HOI perception.

Pose Estimation Schemes. We compare the impact of different pose estimation schemes, as shown in Table 6. We explore two main categories of methods: directly predicting hand joint positions from the hand features and indirectly estimating them by combining reference points and offsets. When directly predicting (row a), we observe that both mAP₅₀ and Full mAP are the lowest among the four schemes. The challenge with this scheme is that it is equivalent to predicting the offsets using the upper left corner of the image as a reference point. The long distance between the reference point and the hand makes accurate prediction extremely difficult.

Various schemes for computing reference points are evaluated, ranging from learnable points to hand box centers and top centers. Compared to direct prediction, leveraging hand-detection-specific features to infer reference points (row b) significantly improves Full mAP by 0.9%. However, the notable improvement in Full mAP is not synchronously reflected in the other two metrics. In contrast, using the centers (row c) or top centers (row d) of the predicted hand boxes as references achieve better results in terms of mAP₅₀. The best performance is achieved using the top



Figure 6: Qualitative comparison between the baseline and our proposed method. For each image, the detection outputs of our proposed method are marked in green, while the baseline outputs are marked in red. The predicted classes and scores are presented in the captions. If no true positive is predicted, the score is marked as **none**. For clarity, the hand category is omitted from the image captions.

Table 7

Performance comparison of different number of selected pose proposal pairs.

# Selected Pose Proposal Pairs (K)	mAP ₅₀	Full	Top@G Acc.
1	84.1	66.8	85.7
2	83.6	66.0	85.7
3	82.5	65.4	82.0
4	83.6	66.4	81.8

center reference points, with mAP₅₀ increased to 84.1%, Full mAP increased to 66.8%, and Top@G Accuracy reaching 85.7%. These improvements are likely due to our ability to explicitly constrain the reference points and estimated joint positions to the vicinity of the hand, leading to more stable and accurate joint localization and further enhancing the overall Ego-HOI detection performance.

Number of Selected Pose Proposal Pairs. We also study the impact of the number of selected pose proposal pairs on model performance. Specifically, we test different values of K (1, 2, 3, and 4), where K represents that only the top K pairs of left-hand and right-hand pose proposals with highest scores are used to extract hand geometric features. The results are summarized in Table 7. Our observations show that the model performs best when $K = 1$. We speculate that increasing the number of proposal pairs may introduce more invalid or low-quality geometric features, which dilutes the effective information and negatively impacts the stability of relational reasoning.

5.6. Qualitative Results and Discussions

To qualitatively demonstrate the advantages of our method in Ego-HOI detection, comparison examples between the baseline and our proposed method are provided in Fig. 6. Our method is particularly outstanding in improving the

confidence of interaction predictions. For instance, in Case 1, the baseline model predicts a *right-hand reach out drawer* with a score of 0.299, while our model significantly improves this score to 0.936. Furthermore, our method successfully recognizes Ego-HOI triplets that the baseline method fails to output a true positive prediction (Cases 7 and 8). These improvements cover scenes with small or occluded objects (Samples 4, 6, 7, 8) and complex scenes (Samples 2, 5, 8), showcasing that our approach can provide more accurate predictions under challenging conditions. Overall, our method shows apparent advantages in prediction accuracy and robustness.

We also compare our proposed method with the baseline across different object occlusion ratios. For Ego-HOI detection, we count prediction results according to their ground truth occlusion ratios, as shown in Fig. 7 (top). For interaction recognition, we statistically classify each prediction according to the average ground truth occlusion ratio of the instances within each image, as shown in Fig. 7 (bottom). Overall, the performance of both the baseline and our method shows a downward trend with the increase of occlusion ratio. This phenomenon occurs because occlusions may obscure critical features, thus hindering the model's learning. Nonetheless, our method consistently outperforms the baseline at all occlusion levels. In particular, at the high occlusion level (0.8~1), our method improves Full mAP by 5.7% and Top@G Accuracy by 4.0% compared to the baseline. These significant improvements are mainly due to our method's ability to leverage poses as additional cues to enhance interaction features and infer interactions more effectively, even when the visible portion of an object is too limited to provide enough information.

6. Conclusion

In this paper, we introduce a new benchmark dataset, Ego-HOIBench, which aims to advance the research of

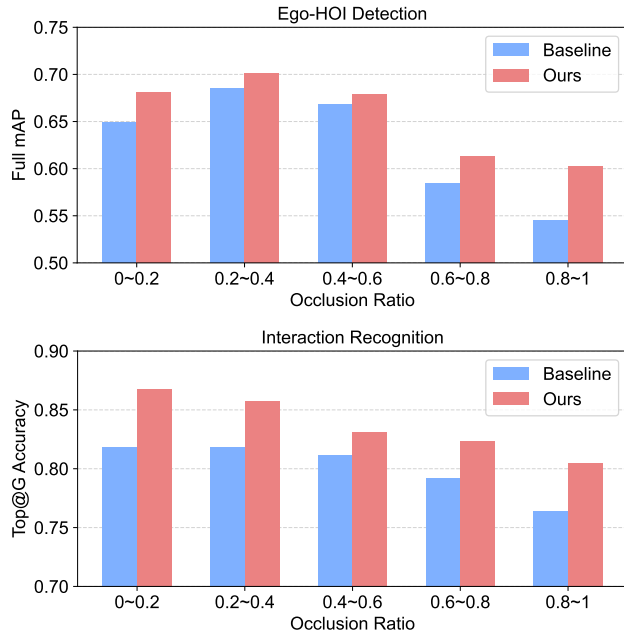


Figure 7: Performance comparison of our proposed method with the baseline for Ego-HOI detection (top) and interaction recognition (bottom) under different object occlusion ratios.

human-object interaction detection from an egocentric perspective. To address the detection challenges exacerbated by severe occlusions in egocentric vision, we propose a Hand Geometric and Interactivity Refinement scheme. Our method ingeniously extracts detailed hand geometric features and utilizes pose offsets prompts to refine interaction features. By fusing these complementary features, it generates more informative and contextual representations for interaction recognition. Importantly, our module can be easily integrated into existing HOI detection frameworks, making it a general and versatile solution. Extensive experiments on the Ego-HOIBench dataset demonstrate the effectiveness of our proposed approach. It significantly improves the accuracy and robustness of interaction recognition and detection compared to various baseline methods. We believe the insights from this work will inspire future research to further enhance real-world applications involving human-object interactions.

Acknowledgements

The research work was conducted in the JC STEM Lab of Machine Learning and Computer Vision funded by The Hong Kong Jockey Club Charities Trust.

References

[1] Nagarajan, T., Feichtenhofer, C., Grauman, K., 2019. Grounded human-object interaction hotspots from video, in: Proceedings of the IEEE/CVF International Conference on Computer Vision, pp. 8688–8697.

[2] Nagarajan, T., Grauman, K., 2021. Shaping embodied agent behavior with activity-context priors from egocentric video. *Advances in Neural Information Processing Systems* 34, 29794–29805.

[3] Kotar, K., Mottaghi, R., 2022. Interaction: Embodied adaptive object detection, in: Proceedings of the IEEE/CVF Conference on Computer Vision and Pattern Recognition, pp. 14860–14869.

[4] Wang, X., Kwon, T., Rad, M., Pan, B., Chakraborty, I., Andrist, S., Bohus, D., Feniello, A., Tekin, B., Frujeri, F.V., et al., 2023. Holoassist: an egocentric human interaction dataset for interactive ai assistants in the real world, in: Proceedings of the IEEE/CVF International Conference on Computer Vision, pp. 20270–20281.

[5] Salvato, M., Heravi, N., Okamura, A.M., Bohg, J., 2022. Predicting hand-object interaction for improved haptic feedback in mixed reality. *IEEE Robotics and Automation Letters* 7, 3851–3857.

[6] Masuda, M., Hachiuma, R., Fujii, R., Saito, H., 2020. Unsupervised anomaly detection of the first person in gait from an egocentric camera, in: International Symposium on Visual Computing, Springer, pp. 604–617.

[7] Lee, S.P., Lu, Z., Zhang, Z., Hoai, M., Elhamifar, E., 2024. Error detection in egocentric procedural task videos, in: Proceedings of the IEEE/CVF Conference on Computer Vision and Pattern Recognition, pp. 18655–18666.

[8] Jia, B., Lei, T., Zhu, S.C., Huang, S., 2022. Egotaskqa: Understanding human tasks in egocentric videos. *Advances in Neural Information Processing Systems* 35, 3343–3360.

[9] Di, S., Xie, W., 2024. Grounded question-answering in long egocentric videos, in: Proceedings of the IEEE/CVF Conference on Computer Vision and Pattern Recognition, pp. 12934–12943.

[10] Fan, C., 2019. Egovqa-an egocentric video question answering benchmark dataset, in: Proceedings of the IEEE/CVF International Conference on Computer Vision Workshops, pp. 0–0.

[11] Park, J., Park, J.W., Lee, J.S., 2023. Viplo: Vision transformer based pose-conditioned self-loop graph for human-object interaction detection, in: Proceedings of the IEEE/CVF Conference on Computer Vision and Pattern Recognition, pp. 17152–17162.

[12] Yuan, H., Zhang, S., Wang, X., Albanie, S., Pan, Y., Feng, T., Jiang, J., Ni, D., Zhang, Y., Zhao, D., 2023. Rlipv2: Fast scaling of relational language-image pre-training, in: Proceedings of the IEEE/CVF International Conference on Computer Vision, pp. 21649–21661.

[13] Zheng, S., Xu, B., Jin, Q., 2023. Open-category human-object interaction pre-training via language modeling framework, in: Proceedings of the IEEE/CVF Conference on Computer Vision and Pattern Recognition, pp. 19392–19402.

[14] Ning, S., Qiu, L., Liu, Y., He, X., 2023. Hoiclip: Efficient knowledge transfer for hoi detection with vision-language models, in: Proceedings of the IEEE/CVF Conference on Computer Vision and Pattern Recognition, pp. 23507–23517.

[15] Lei, T., Caba, F., Chen, Q., Jin, H., Peng, Y., Liu, Y., 2023. Efficient adaptive human-object interaction detection with concept-guided memory, in: Proceedings of the IEEE/CVF International Conference on Computer Vision, pp. 6480–6490.

[16] Chen, J., Yanai, K., 2023. Qahoi: Query-based anchors for human-object interaction detection, in: 2023 18th International Conference on Machine Vision and Applications (MVA), IEEE, pp. 1–5.

[17] Kim, B., Mun, J., On, K.W., Shin, M., Lee, J., Kim, E.S., 2022. Mstr: Multi-scale transformer for end-to-end human-object interaction detection, in: Proceedings of the IEEE/CVF Conference on Computer Vision and Pattern Recognition, pp. 19578–19587.

[18] Yuan, H., Wang, M., Ni, D., Xu, L., 2022. Detecting human-object interactions with object-guided cross-modal calibrated semantics, in: Proceedings of the AAAI Conference on artificial intelligence, pp. 3206–3214.

[19] Hou, Z., Yu, B., Tao, D., 2022. Discovering human-object interaction concepts via self-compositional learning, in: European Conference on Computer Vision, Springer, pp. 461–478.

[20] Grauman, K., Westbury, A., Byrne, E., Chavis, Z., Furnari, A., Girdhar, R., Hamburger, J., Jiang, H., Liu, M., Liu, X., et al., 2022. Ego4d: Around the world in 3,000 hours of egocentric video, in:

- Proceedings of the IEEE/CVF Conference on Computer Vision and Pattern Recognition, pp. 18995–19012.
- [21] Damen, D., Doughty, H., Farinella, G.M., Fidler, S., Furnari, A., Kazakos, E., Moltisanti, D., Munro, J., Perrett, T., Price, W., et al., 2018. Scaling egocentric vision: The epic-kitchens dataset, in: Proceedings of the European conference on computer vision (ECCV), pp. 720–736.
 - [22] Damen, D., Doughty, H., Farinella, G.M., Furnari, A., Kazakos, E., Ma, J., Moltisanti, D., Munro, J., Perrett, T., Price, W., et al., 2022. Rescaling egocentric vision: Collection, pipeline and challenges for epic-kitchens-100. *International Journal of Computer Vision*, 1–23.
 - [23] Li, Y., Liu, M., Rehg, J.M., 2018. In the eye of beholder: Joint learning of gaze and actions in first person video, in: Proceedings of the European conference on computer vision (ECCV), pp. 619–635.
 - [24] Sener, F., Chatterjee, D., Shelepov, D., He, K., Singhania, D., Wang, R., Yao, A., 2022. Assembly101: A large-scale multi-view video dataset for understanding procedural activities, in: Proceedings of the IEEE/CVF Conference on Computer Vision and Pattern Recognition, pp. 21096–21106.
 - [25] Ragusa, F., Furnari, A., Farinella, G.M., 2023. Meccano: A multimodal egocentric dataset for humans behavior understanding in the industrial-like domain. *Computer Vision and Image Understanding* 235, 103764.
 - [26] Ohkawa, T., He, K., Sener, F., Hodan, T., Tran, L., Keskin, C., 2023. Assemblyhands: Towards egocentric activity understanding via 3d hand pose estimation, in: Proceedings of the IEEE/CVF Conference on Computer Vision and Pattern Recognition, pp. 12999–13008.
 - [27] Leonardi, R., Ragusa, F., Furnari, A., Farinella, G.M., 2024. Exploiting multimodal synthetic data for egocentric human-object interaction detection in an industrial scenario. *Computer Vision and Image Understanding* 242, 103984.
 - [28] Garcia-Hernando, G., Yuan, S., Baek, S., Kim, T.K., 2018. First-person hand action benchmark with rgb-d videos and 3d hand pose annotations, in: Proceedings of the IEEE conference on computer vision and pattern recognition, pp. 409–419.
 - [29] Kwon, T., Tekin, B., Stühmer, J., Bogo, F., Pollefeys, M., 2021. H2o: Two hands manipulating objects for first person interaction recognition, in: Proceedings of the IEEE/CVF International Conference on Computer Vision, pp. 10138–10148.
 - [30] Liu, Y., Liu, Y., Jiang, C., Lyu, K., Wan, W., Shen, H., Liang, B., Fu, Z., Wang, H., Yi, L., 2022. Hoi4d: A 4d egocentric dataset for category-level human-object interaction, in: Proceedings of the IEEE/CVF Conference on Computer Vision and Pattern Recognition, pp. 21013–21022.
 - [31] Tekin, B., Bogo, F., Pollefeys, M., 2019. H+ o: Unified egocentric recognition of 3d hand-object poses and interactions, in: Proceedings of the IEEE/CVF conference on computer vision and pattern recognition, pp. 4511–4520.
 - [32] Tu, D., Sun, W., Zhai, G., Shen, W., 2023. Agglomerative transformer for human-object interaction detection, in: Proceedings of the IEEE/CVF international conference on computer vision, pp. 21614–21624.
 - [33] Rajasegaran, J., Pavlakos, G., Kanazawa, A., Feichtenhofer, C., Malik, J., 2023. On the benefits of 3d pose and tracking for human action recognition, in: Proceedings of the IEEE/CVF Conference on Computer Vision and Pattern Recognition, pp. 640–649.
 - [34] Qiao, T., Men, Q., Li, F.W., Kubotani, Y., Morishima, S., Shum, H.P., 2022. Geometric features informed multi-person human-object interaction recognition in videos, in: European Conference on Computer Vision, Springer. pp. 474–491.
 - [35] Li, Y.L., Liu, X., Wu, X., Huang, X., Xu, L., Lu, C., 2022. Transferable interactivity knowledge for human-object interaction detection. *IEEE Transactions on Pattern Analysis & Machine Intelligence* 44, 3870–3882.
 - [36] Zheng, S., Chen, S., Jin, Q., 2020. Skeleton-based interactive graph network for human object interaction detection, in: 2020 IEEE International Conference on Multimedia and Expo (ICME), IEEE. pp. 1–6.
 - [37] Gupta, T., Schwing, A., Hoiem, D., 2019. No-frills human-object interaction detection: Factorization, layout encodings, and training techniques, in: Proceedings of the IEEE/CVF International Conference on Computer Vision, pp. 9677–9685.
 - [38] Wan, B., Zhou, D., Liu, Y., Li, R., He, X., 2019. Pose-aware multi-level feature network for human object interaction detection, in: Proceedings of the IEEE/CVF International Conference on Computer Vision, pp. 9469–9478.
 - [39] Liu, Q., Che, X., Zhao, M., Xu, H., Li, Y., 2024. Cktn: Commonsense knowledge transfer network for human activity understanding. *Knowledge-Based Systems* 286, 111427.
 - [40] Zhang, L., Zhou, S., Stent, S., Shi, J., 2022b. Fine-grained egocentric hand-object segmentation: Dataset, model, and applications, in: European Conference on Computer Vision, Springer. pp. 127–145.
 - [41] Ma, Z., Zhang, F., Nan, Z., Ge, Y., 2024. Intention action anticipation model with guide-feedback loop mechanism. *Knowledge-Based Systems* 292, 111626.
 - [42] Zhang, S., Ma, Q., Zhang, Y., Qian, Z., Kwon, T., Pollefeys, M., Bogo, F., Tang, S., 2022c. Egobody: Human body shape and motion of interacting people from head-mounted devices, in: European conference on computer vision, Springer. pp. 180–200.
 - [43] Gao, C., Xu, J., Zou, Y., Huang, J.B., 2020. Drg: Dual relation graph for human-object interaction detection, in: Computer Vision–ECCV 2020: 16th European Conference, Glasgow, UK, August 23–28, 2020, Proceedings, Part XII 16, Springer. pp. 696–712.
 - [44] Zhang, F.Z., Yuan, Y., Campbell, D., Zhong, Z., Gould, S., 2023. Exploring predicate visual context in detecting of human-object interactions, in: Proceedings of the IEEE/CVF International Conference on Computer Vision, pp. 10411–10421.
 - [45] Zhang, F.Z., Campbell, D., Gould, S., 2022a. Efficient two-stage detection of human-object interactions with a novel unary-pairwise transformer, in: Proceedings of the IEEE/CVF Conference on Computer Vision and Pattern Recognition, pp. 20104–20112.
 - [46] Zhang, Y., Pan, Y., Yao, T., Huang, R., Mei, T., Chen, C.W., 2022d. Exploring structure-aware transformer over interaction proposals for human-object interaction detection, in: Proceedings of the IEEE/CVF Conference on Computer Vision and Pattern Recognition, pp. 19548–19557.
 - [47] Z. Zhang, F., Campbell, D., Gould, S., 2021. Spatially conditioned graphs for detecting human-object interactions, in: Proceedings of the IEEE/CVF International Conference on Computer Vision, pp. 13319–13327.
 - [48] Yang, D., Zou, Y., Li, Z., Li, G., 2021. Learning human-object interaction via interactive semantic reasoning. *IEEE Transactions on Image Processing* 30, 9294–9305.
 - [49] Ren, S., He, K., Girshick, R., Sun, J., 2016. Faster r-cnn: Towards real-time object detection with region proposal networks. *IEEE transactions on pattern analysis and machine intelligence* 39, 1137–1149.
 - [50] Carion, N., Massa, F., Synnaeve, G., Usunier, N., Kirillov, A., Zagoruyko, S., 2020. End-to-end object detection with transformers, in: European conference on computer vision, Springer. pp. 213–229.
 - [51] Liao, Y., Liu, S., Wang, F., Chen, Y., Qian, C., Feng, J., 2020. Ppdm: Parallel point detection and matching for real-time human-object interaction detection, in: Proceedings of the IEEE/CVF Conference on Computer Vision and Pattern Recognition, pp. 482–490.
 - [52] Kim, B., Lee, J., Kang, J., Kim, E.S., Kim, H.J., 2021. Hotr: End-to-end human-object interaction detection with transformers, in: Proceedings of the IEEE/CVF conference on computer vision and pattern recognition, pp. 74–83.
 - [53] Kim, B., Choi, T., Kang, J., Kim, H.J., 2020. Uniondet: Union-level detector towards real-time human-object interaction detection, in: Computer Vision–ECCV 2020: 16th European Conference, Glasgow, UK, August 23–28, 2020, Proceedings, Part XV 16, Springer. pp. 498–514.
 - [54] Kim, S., Jung, D., Cho, M., 2023. Relational context learning for human-object interaction detection, in: Proceedings of the IEEE/CVF

- Conference on Computer Vision and Pattern Recognition, pp. 2925–2934.
- [55] Lin, W.K., Zhang, H.B., Fan, Z., Liu, J.H., Yang, L.J., Lei, Q., Du, J., 2023. Point-based learnable query generator for human–object interaction detection. *IEEE Transactions on Image Processing* 32, 6469–6484.
 - [56] Tamura, M., Ohashi, H., Yoshinaga, T., 2021. Qpic: Query-based pairwise human-object interaction detection with image-wide contextual information, in: *Proceedings of the IEEE/CVF Conference on Computer Vision and Pattern Recognition*, pp. 10410–10419.
 - [57] Li, T., Geng, P., Lu, X., Li, W., Lyu, L., 2024. Skeleton-based action recognition through attention guided heterogeneous graph neural network. *Knowledge-Based Systems* , 112868.
 - [58] Wu, X., Li, Y.L., Liu, X., Zhang, J., Wu, Y., Lu, C., 2022. Mining cross-person cues for body-part interactiveness learning in hoi detection, in: *European Conference on Computer Vision*, Springer. pp. 121–136.
 - [59] Dong, L., Li, Z., Xu, K., Zhang, Z., Yan, L., Zhong, S., Zou, X., 2022. Category-aware transformer network for better human-object interaction detection, in: *Proceedings of the IEEE/CVF Conference on Computer Vision and Pattern Recognition*, pp. 19538–19547.
 - [60] Rezaatofghi, H., Tsoi, N., Gwak, J., Sadeghian, A., Reid, I., Savarese, S., 2019. Generalized intersection over union: A metric and a loss for bounding box regression, in: *Proceedings of the IEEE/CVF conference on computer vision and pattern recognition*, pp. 658–666.
 - [61] Lin, T.Y., Goyal, P., Girshick, R., He, K., Dollár, P., 2017. Focal loss for dense object detection, in: *Proceedings of the IEEE international conference on computer vision*, pp. 2980–2988.